Title

Tuning Zr6 Metal–Organic Framework (MOF) Nodes as Catalyst Supports: Site Densities and Electron-Donor Properties Influence Molecular Iridium Complexes as Ethylene Conversion Catalysts

Journal

ACS Catalysis, 6(1)

ISSN

2155-5435

Authors

Yang, Dong
Odoh, Samuel O
Borycz, Joshua
et al.

Publication Date

2016-01-04

DOI

10.1021/acscatal.5b02243

Peer reviewed

Tuning Zr_6 MOF Nodes as Catalyst Supports: Site Densities and Electron-Donor Properties Influence Molecular Iridium Complexes as Ethylene Conversion Catalysts

Dong Yang,[a] Samuel O. Odoh,[b] Joshua Borycz,[b] Timothy C. Wang,[c] Omar K. Farha,[c,d] Joseph T. Hupp,[c] Christopher J. Cramer,[b] Laura Gagliardi,[b*] Bruce C. Gates[a*]

[a] Department of Chemical Engineering & Materials Science, University of California, Davis, California 95616, United States

[b] Department of Chemistry, Chemical Theory Center, and Supercomputing Institute, University of Minnesota, Minneapolis, Minnesota 55455-0431, United States

[c] Department of Chemistry, Northwestern University, 2145 Sheridan Road, Evanston, Illinois 60208, United States

[d] Department of Chemistry, Faculty of Science, King Abdul-Aziz University, Jeddah 22254, Saudi Arabia

ABSTRACT: The Zr_6 nodes of the metal organic frameworks (MOFs) UiO-66 and UiO-67 are metal oxide clusters of atomic precision and can be used as catalyst supports. The bonding sites on these nodes, that is, hydrogen-bonded H_2O/OH groups on UiO-67 and non-hydrogen-bonded terminal OH groups on UiO-66, were regulated by modulation of the MOF syntheses. $Ir(C_2H_4)_2(C_5H_7O_2)$ complexes reacted with these sites to give site-isolated $Ir(C_2H_4)_2$ complexes, each anchored to the node by two Ir–O_{node} bonds. The supported iridium complexes on these sites have been characterized by infrared (IR) and extended X-ray absorption fine structure spectroscopies and density functional theory calculations. The ethylene ligands on iridium are readily replaced by CO, and the ν_{CO} frequencies of the resultant complexes and those of comparable complexes reported elsewhere show that the support electron-donor tendencies increase in the order zeolite HY << UiO-66 < UiO-67 (= NU-1000) < ZrO_2 < MgO. The sharpness of the IR ν_{CO} bands shows that the degree of uniformity of the support bonding sites decreases in the order ZrO_2 ≈ UiO-67 ≈ NU-1000 < MgO < UiO-66 << HY zeolite. The reactivity of supported $Ir(CO)_2$ complexes with C_2H_4 to form $Ir(C_2H_4)(CO)$ and $Ir(C_2H_4)_2(CO)$ is influenced by the support electron-donor properties, with the reactivity increasing in the order MgO = ZrO_2 = NU-1000 (not reactive) < UiO-66 < UiO-67 << HY zeolite. DFT calculations characterizing the complexes supported on NU-1000, UiO-66/67, and HY zeolite concur with the use of the calculated ν_{CO} bands as indicators of electron-donor properties of the supported metal catalysts. Our calculations also show that the reactivity of the supported $Ir(CO)_2$ complexes with C_2H_4 is correlated with the electron-donor properties of the iridium center. The supported $Ir(C_2H_4)_2$ samples are precatalysts for ethylene hydrogenation and ethylene dimerization, with the activity for each reaction increasing with increasing electron-withdrawing strength of the support.

KEYWORDS: *metal organic framework nodes; catalyst supports; iridium ethylene complexes; iridium carbonyl complexes; ethylene hydrogenation; ethylene dimerization*

INTRODUCTION

Thermally stable metal-organic frameworks (MOFs) offer excellent but still little-explored prospects as catalyst supports.[1-10] Catalysts can be bonded to either the organic MOF linkers[11-13] or to the MOF nodes,[14-17] some of which are essentially small pieces of metal oxides. Such nodes are roughly comparable to conventional metal oxide catalyst supports, but, in contrast to porous metal oxides, they are nearly uniform in structure and offer unique opportunities for precise tuning of their properties to influence catalyst performance.

MOF nodes that offer such opportunities include the $[Zr_6(\mu_3\text{-}O)_4(\mu_3\text{-}OH)_4(OH)_4(OH_2)_4]^{8+}$ and $[Zr_6(\mu_3\text{-}O)_4(\mu_3\text{-}OH)_4]^{12+}$ nodes that occur in NU-1000 and UiO-66, respectively. The functional groups (e.g., OH and OH_2 groups) on these nodes provide anchoring sites for metals, and our goals were to determine how to vary the properties of catalysts supported on them and to lay a foundation for design of MOF-supported catalysts. We investigated

structurally simple and essentially molecular metal catalysts on a family of MOF nodes and determined how their structures influence metal–support bonding and catalytic properties for a simple test reaction, ethylene conversion in the presence of H_2. We also sought to compare the MOF nodes with conventional catalyst supports. The strategy was to synthesize MOF node-supported metal complex catalysts precisely by using an organometallic precursor and to characterize them with complementary experimental and theoretical approaches. The MOFs UiO-66 and UiO-67 were chosen because they (and their nodes) have been well characterized[18-20] and because they can be used as supports for metal complexes made from precursors such as $Ir(C_2H_4)_2(acac)$ (acac is acetylacetonate) to give catalysts that are suitable for precise characterization.

IR spectroscopy and density functional theory (DFT) calculations were used previously in an investigation of the reactions of OH groups on the nodes of the MOFs NU-1000 and UiO-66. In that work, catalysts bonded to the MOF nodes were made from the precursors $Ir(C_2H_4)_2(acac)$ and $Ir(CO)_2(acac)$.[17] In the work reported here, the MOF syntheses were varied by the choice of modulators to influence the number of node defect sites associated with missing linkers and thereby to vary the properties of the MOFs as catalyst supports. For example, UiO-66 was synthesized with the modulator acetic acid so that the MOF had approximately 1 of 12 linkers per node missing.[22] The nodes of UiO-66 modulated by acetic acid incorporate hydrogen-bonded H_2O/OH surface groups (labeled as **site 1** in Scheme 1) and non-hydrogen-bonded OH groups (labeled as **site 2** in Scheme 1). We also synthesized UiO-66 and UiO-67 with various numbers of node defect sites (up to ~4 of 12 missing linkers per node) by also using HCl as a modulator.[20]

Our results show that the synthesis conditions can be chosen to generate essentially one type of bonding site on each MOF node—that is, **site 1** on UiO-67 and **site 2** on UiO-66. Moreover, the DFT calculations show that the influences of the nodes as ligands of the iridium complex catalysts are dictated by their electron-donor properties, which allows comparisons with conventional catalyst supports.

EXPERIMENTAL METHODS

Synthesis of UiO-66 with HCl Modulator. $ZrCl_4$ (99.99%, 0.125 g, 0.54 mmol) and 1 mL of concentrated HCl (modulator, 37 wt %) were dissolved in 15 mL of dimethylformamide (DMF) in an 8-dram vial by using ultrasound for 5 min. The linker precursor benzene-1,4-dicarboxylic acid (0.123 g, 0.75 mmol) was then added into the solution and dissolved by ultrasound applied for about 15 min. The vials were kept in an oven at 353 K under static conditions for 24 h. White precipitates were produced, and they were isolated by centrifugation after cooling to room temperature. The solids were washed with DMF three times to remove unreacted precursors and with methanol six times to remove DMF. Then the powder was dried at room temperature.

Synthesis of UiO-67 with HCl Modulator. $ZrCl_4$ (0.067 g, 0.27 mmol) and 0.5 mL of concentrated HCl (modulator, 37 wt %) were dissolved in 15 mL of DMF in an 8 dram vial by using ultrasound for 5 min. Biphenyl-4,4'-dicarboxylic acid (0.09 g, 0.38 mmol) was then added to the solution and dispersed by ultrasound applied for about 15 min. The vials were kept in an oven at 353 K under static conditions for 24 h. A white precipitate formed, and it was isolated by centrifugation after cooling to room temperature. The solid was washed with DMF three times to remove unreacted precursors and with acetone six times to remove DMF. Then the powder was dried at room temperature.

Synthesis of UiO-67 with Acetic Acid Modulator. $ZrCl_4$ (0.12 g, 0.48 mmol) and 1.0 mL of acetic acid (modulator) were dissolved in 20 mL of DMF in an 8 dram vial by using ultrasound for 5 min. Biphenyl-4,4'-dicarboxylic acid (0.125 g, 0.53 mmol) was then added to the solution and dispersed by ultrasound applied for about 15 min. The vials were kept in an oven at 393 K under static conditions for 24 h. A white precipitate formed, and it was isolated by centrifugation after cooling of the sample to room temperature. The solid was washed with DMF three times to remove unreacted precursors and with acetone six times to remove DMF. Then the powder was dried at room temperature.

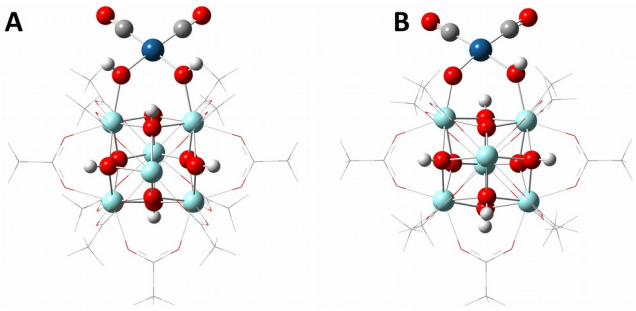

Scheme 1. The missing linker sites in UiO-66 can be occupied by either (A) a H_2O/OH terminal pair (**site 1**) or by (B) two OH terminal pairs with a migrated proton at another portion of the node (**site 2**). In these figures, one of the terminal protons is replaced by an Ir(I) dicarbonyl complex.

Synthesis of MOF-supported $Ir(C_2H_4)_2$. Sample synthesis and handling were performed with the exclusion of moisture and air by use of a double-manifold Schlenk vacuum line and an argon-atmosphere glove box. The precursor $Ir(C_2H_4)_2(acac)$ was synthesized as described elsewhere;[23] it has been characterized by X-ray diffraction crystallography and ^1H and ^{13}C NMR, Raman, and IR spectroscopies.[23]

Each supported iridium complex was prepared by bringing $Ir(C_2H_4)_2(acac)$ (36.2 mg for a 10.0 wt % iridium loading or 3.6 mg for a 1.0 wt % iridium loading) in contact with 200 mg of activated MOF

powder (UiO-66 or UiO-67, activated under vacuum (10^{-7} Torr) at 423 or 393 K, respectively, for 24 h before use) in a Schlenk flask. The mixture was slurried in 30 mL of dried *n*-pentane (Fisher, 99%) at room temperature. After 8 h, the solvent was removed by evacuation for a day, leaving all the iridium bonded to the MOF. The resultant solids (e.g. that containing 10.0 wt % iridium, with approximately 1 Ir atom per node), was stored in an argon-filled glovebox.

Iridium loadings were inferred from the conditions of the syntheses, whereby all the added iridium remained in the MOF after removal of the solvent. The catalysts with 1.0 wt % iridium loadings were used only for catalytic activity measurements, and those with 10.0 wt % iridium loading were used for all other characterizations.

Synthesis of ZrO_2 and ZrO_2-supported $Ir(C_2H_4)_2$. The amorphous metal oxide support ZrO_2 was synthesized by a precipitation method. $ZrO(NO_3)_2{\cdot}xH_2O$ (99.99%, 3.64 g, 15.74 mmol) and 28.9 mL of concentrated HNO_3 (65 wt %) were dissolved in 1 L of de-ionized water by stirring for 30 min. Ammonium hydroxide solution (100 mL, 28% NH_3 in water) was then added dropwise to the solution with vigorous stirring, and the final pH value was controlled to be 9–10. The resultant suspension was aged for 4 h by continuous stirring followed by filtration. The precipitate was washed 6 times with deionized water to give a neutral pH value and then dried at 393 K overnight. The powder was calcined at 773 K in O_2 for 2 h and evacuated at 773 K for 12 h.

To prepare the ZrO_2-supported iridium complex, $Ir(C_2H_4)_2(acac)$ (18.1 mg) and the calcined ZrO_2 powder (1.0 g) in a Schlenk flask were combined into a slurry in dried *n*-pentane (30 mL) at room temperature. After 24 h, the solvent was removed by evacuation for 24 h so that all of the iridium remained on the support. The resultant solid, containing 1.0 wt % iridium, was stored in the glovebox.

BET Measurements. All N_2 isotherms were measured with a Micromeritics Tristar II instrument. Measurements were performed at 77 K, with the temperature held constant with a liquid nitrogen bath. Consistency criteria were adapted to choose an appropriate pressure range for BET surface area calculations.

Infrared Spectroscopy. A Bruker IFS 66v/S spectrometer with a spectral resolution of 2 cm^{-1} was used to collect transmission IR spectra of power samples. Approximately 30 mg of solid sample in the glovebox was pressed into a thin wafer and loaded into a cell that was also a flow reactor (In-situ Research Institute, South Bend, IN). The cell was sealed and connected to a flow system, and spectra were recorded while reactant gases flowed through the cell at various temperatures. Each spectrum is the average of 64 scans.

X-ray Absorption Spectroscopy. X-ray absorption spectra were collected at X-ray beamline 2-2 of the Stanford Synchrotron Radiation Lightsource (SSRL). The storage ring electron energy was 3 GeV, and the ring current was approximately 300 mA. A double-crystal Si(220) monochromator was detuned by 20−25% at the Ir L_{III} edge to minimize the effects of higher harmonics in the X-ray beam. Samples were transferred to the X-ray absorption spectroscopy cells in an inert atmosphere glovebox and sealed before mounting in the X-ray beam.

Catalytic Reaction Experiments. Ethylene hydrogenation catalysis was carried out in a conventional laboratory once-through tubular plug-flow reactor at 298 K and 1 bar. The catalyst (10–50 mg) was mixed with 10 g of inert, nonporous α-Al_2O_3 powder and loaded into the reactor in the argon-filled glovebox. The feed partial pressures were 100 mbar of C_2H_4, 200 mbar of H_2, and 700 mbar of helium, with a total flow rate of 100 mL(NTP)/min. Products were analyzed with an online Agilent 6890 gas chromatograph. The ethylene conversions were <5%, and the reactor was well approximated as differential, determining reaction rates directly.

COMPUTATIONAL METHODS

We used the same computational models that we previously applied[17] to some of these systems, and which have also been used to predict the structural properties of many other MOFs as well as their behavior as gas adsorbents, catalysts, catalyst supports, and optical materials[24]. Specifically, periodic DFT calculations were carried out with the PBE[25] exchange-correlation functional augmented with dispersion correction terms, PBE-D3[26] to model the entire materials. For UiO-66/67, one linker was removed from each of the periodic unit cells, in order to describe the terminal H_2O/OH and OH/OH sites crucial for chemisorbing iridium complexes. For NU-1000, there was no need to perform this modification, as its Zr_6 nodes naturally have terminal H_2O/OH groups. The periodic DFT calculations were carried out with the VASP 5.3.3 package using plane wave basis sets, the projector augmented wave (PAW[29]) method for describing electron-ion interactions, an energy cutoff of 550 eV, and 1 × 1 × 1 Monkhorst-Pack K-point meshes.

The Zr_6 nodes of NU-1000 and UiO-66/67 were subsequently modeled as finite clusters that were extracted from optimized periodic unit cells to allow investigation of the details of the supported iridium complexes. The cluster models were obtained from the optimized periodic unit cells by truncating the organic linkers to benzoate (C_6H_5-COO^-) and acetate (CH_3COO^-) groups, for NU-1000 and UiO66/67, respectively. These types of models have been shown to properly describe the nature of the terminal water or hydroxyl groups on the Zr_6 nodes of NU-1000 as well as the catalytic properties of species bonded to the nodes of this MOF. The cluster models were optimized using the M06-L[31] density functional, the def2-svp basis set for C, H, and O atoms, and the def2-

tzvpp[32-34] basis sets with associated effective core potentials for Zr and Ir atoms. In all cases, the positions of all atoms were optimized, except for the C and H atoms of the benzoate groups used in the cluster model of NU-1000. For UiO-66/67, all atoms were allowed to move during geometry optimizations. The optimizations were carried out without symmetry constraints and until tight energy and geometry convergence criteria were attained; ultrafine grids were used.

For calculations characterizing HY zeolite, we used the same basis sets, grids, and geometry and energy convergence criteria that were used in the calculations characterizing the MOFs. We use a 33T cluster model that consists of 13 interconnected four-ring systems that face the supercage of the zeolite. A sodalite cage and 2 $SiO_2(OH)_2$ groups were added to complete the ring of the cluster model, Scheme 2. In all cases, we used protons to cap dangling Si-O bonds. This cluster model was obtained from a periodic structure optimized with the PBE-D3 functional while using plane wave basis sets, as was done for the MOFs.

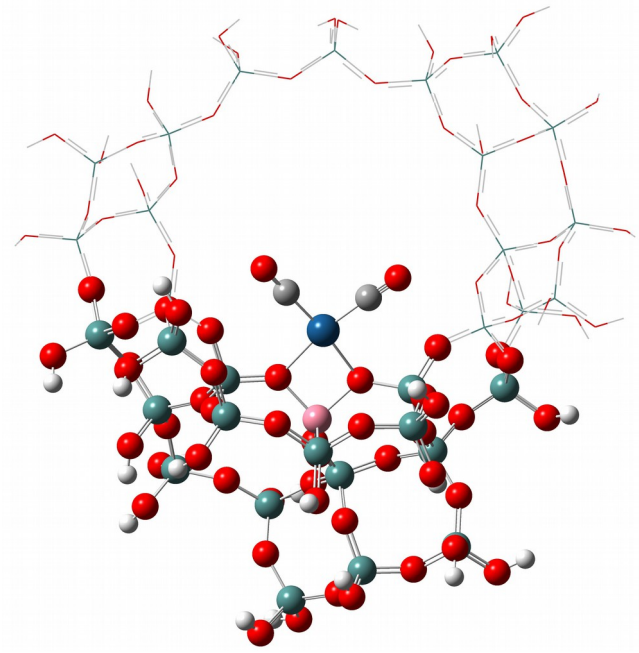

Scheme 2. The 33T cluster model used in calculations on HY zeolite. The Zr, Ir, Si, O, C, and H atoms are shown as light blue, dark blue, green, red, gray, and white spheres, respectively. Only the atoms near the deposited $Ir(CO)_2$ complex are shown. The rest are represented by wireframes.

RESULTS

Defect Sites in UiO-66 and UiO-67 Resulting from Modulation of Syntheses by HCl and by Acetic Acid. The sites on MOF nodes for bonding of catalysts are influenced by the number of missing linkers, which is influenced by modulators in the MOF syntheses. The quantification of the missing linkers in UiO-66 and UiO-67 samples has been performed by thermal gravimetric analysis (TGA) with samples under an O_2 atmosphere.[20] Assuming that the residual mass of the samples corresponds to the zirconium content in the MOFs, one can calculate the theoretical mass loss (from the loss of the linkers) for "defect-free" samples. The actual mass loss that was measured was compared with this value so the number of missing linkers could be quantified.

The TGA data (Table 1) show that approximately 1.4 and 1.2 of the 12 node linkers were missing from the HCl-modulated UiO-66 and UiO-67, respectively, and only ~0.9 and 0.6 of the 12 node linkers were missing from acetic acid-modulated UiO-66 and UiO-67, respectively. Our data are consistent with reported data[20] showing that MOFs modulated by HCl have almost twice as many missing linker sites as MOFs modulated by acetic acid.

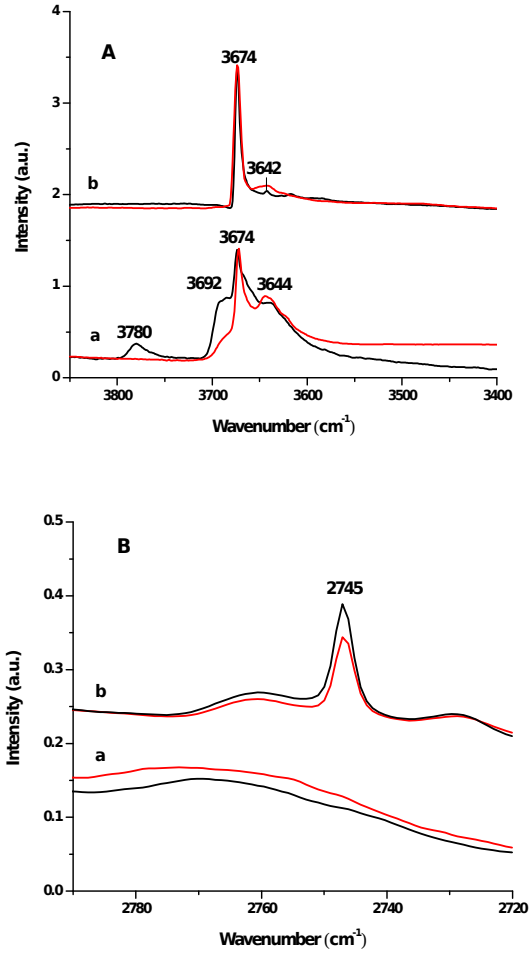

Figure 1. IR spectra characterizing the (A) OH region and (B) hydrogen-bonded H_2O and OH regions characterizing (a) bare UiO-66 and (b) bare UiO-67 (black) and the samples formed by adsorption of $Ir(C_2H_4)_2(acac)$ on them (red).

Table 1. Comparison of bonding sites on Zr_6 nodes of UiO-66 and UiO-67 synthesized with different modulators and having different types of defect sites generated on the nodes.

MOF	Modulator	Number of missing linkers per node[a]	Bonding sites for metal complexes[b]	Ref.
UiO-66	acetic acid	0.9	**sites 1** and **2**	[17]
	HCl	1.4	**site 2**	this work
UiO-67	acetic acid	0.6	**site 1**	this work
	HCl	1.2	**site 1**	this work

[a]Each Zr_6 node is bonded to 12 linkers at a maximum. [b]Site 2 is characterized by IR bands at 3780 and 3692 cm^{-1}, site 1 by a band at 2745 cm^{-1}.

Furthermore, the IR band intensities of the hydroxyl groups at missing linker sites (3780, 3692, and 2745 cm^{-1}) are much greater for the MOFs modulated with HCl than those modulated with acetic acid (Figure 1, Figure S1). The non-hydrogen bonded OH bands at 3780 and 3692 cm^{-1}, which characterize **site 2** on HCl-modulated UiO-66 (Figure 1A), are more intense than previously reported hydroxyl bands characterizing **site 2** of acetic acid-modulated UiO-66,[17] indicating that more bonding sites are generated by using HCl as the modulator rather than acetic acid. The hydrogen-bonded H_2O/OH band characterizing UiO-67 (at 2745 cm^{-1} (**site 1**)) was also found to be more intense when HCl was used as the modulator (Figure 1B) rather than acetic acid (Figure S1B).

The samples with various defect site densities provide an essential opportunity to vary the loading of catalytically active iridium complexes on the nodes.

The IR spectra show that the missing linker sites on HCl-modulated UiO-66 were covered by non-hydrogen-bonded OH groups (**site 2**, Figure 1A). The lack of a band near 2745 cm^{-1} indicates the absence of hydrogen-bonded OH groups on this MOF.

On the other hand, samples with only **site 1** were generated on the nodes of UiO-67 modulated by either HCl or acetic acid, as evidenced by the sharp band (with HCl modulator, Figure 1B) and the weak band (with acetic acid modulator, Figure S1B), each at 2745 cm^{-1}, with both spectra lacking bands at 3780 and 3692 cm^{-1} (Figure 1A and Figure S1A); these results indicate the absence of non-hydrogen bonded OH groups on this MOF.

Thus, UiO-66 and UiO-67 were prepared, each with only one type of site for metal bonding, offering the opportunity for preparation of unique supported metal complexes, thereby facilitating precise structure determinations and allowing a comparison of the two MOFs as catalyst supports. The key results comparing the MOFs are summarized in Table 1.

DFT calculations representing the cluster model of UiO-66/67 predict the O–H stretching of the hydrogen-bonded OH group of site 1 at 2805.2 cm^{-1}, compared with the experimental value of 2745 cm^{-1}. This comparison suggests that a scaling factor of about 0.979 is appropriate for hydrogen-bonded OH groups. The other O–H stretching modes (mainly of μ_3-OH groups) were calculated to have frequencies of about 3872 and 3899 cm^{-1}. These also overestimate the experimental values, 3642 and 3674 cm^{-1}, respectively (Figure 1). This comparison suggests that a scaling factor of about 0.94–0.98 is needed for the calculated vibrational frequencies. The values of these scaling factors lead us to suggest that a single value might not account satisfactorily for the relative contributions of anharmonic effects in hydrogen-bonded and non-hydrogen-bonded OH groups. Nonetheless, the predicted splitting between the calculated μ_3-OH stretching frequencies at 3872 and 3899 cm^{-1} (27 cm^{-1}) matches the measured splitting well: 3642 and 3674 cm^{-1} (32 cm^{-1}).

The calculations for **site 2** predict the μ_3-OH stretching modes at approximately 3869 and 3901 cm^{-1}, similar to the values for **site 1**. There is, however, no hydrogen-bonded OH group in the **site 2** structure and thus no peak in the region near 2700–2800 cm^{-1}.

Bonding of Iridium Complex to Surface Sites on UiO-66 and UiO-67 Nodes. Samples prepared from $Ir(C_2H_4)_2(acac)$ and the MOFs UiO-66 and UiO-67 made with HCl modulation and UiO-67 made with acetic acid modulation were characterized by IR and EXAFS spectroscopies and DFT calculations. The results show that the iridium complexes reacted with hydroxyl groups on the nodes, as shown by the decreased intensities of the O–H bands at 3780 and 3692 cm^{-1} in the IR spectra of Figure 1A characterizing UiO-66 made with the HCl modulator, UiO-66(HCl), and the O–H–O band at 2745 cm^{-1} characterizing UiO-67(HCl) in Figure 1B and UiO-67(acetic acid) in Figure S1B. The chemisorption reactions were accompanied by the removal of acac ligands from the iridium, as shown by the lack of the shells associated with acac ligands in the EXAFS data (Table 2). We infer that acac was converted to Hacac on the basis of reported results characterizing the reaction between the precursor and HY zeolite, which showed that an IR band at 1537 cm^{-1}, assigned as $\nu_{as}(CCC)_{ring}$ of Hacac, appeared after the reaction.[36] However, this band was not distinguishable in the spectra of our MOF samples because of the strong interfering absorption by the organic linkers. DFT calculations characterizing the NU-1000 cluster model show that the region near 1638–1668 cm^{-1} includes intense vibrations assigned to the asymmetric stretching of the C–O bonds of the carboxylate groups of the organic ligands, $\nu_{as}(OCO)$ (see the Supporting Information for details). Application of a scaling factor of 0.941, to the region around 1638–1668 cm^{-1} obtained for

the non-hydrogen bonded OH groups, brings it near 1541-1570 cm^{-1}, explaining our inability to distinguish the $\nu_{as}(CCC)_{ring}$ of Hacac in our MOF samples.

The iridium became bonded to the nodes of UiO-66 and UiO-67, as shown by the EXAFS data indicating an $Ir–O_{support}$ coordination number of nearly 2 (EXAFS data were recorded for UiO-67 and NU-1000, but not UiO-66, Table 2) and consistent with DFT calculations.

The calculated structural properties of $Ir(C_2H_4)_2$ supported at **site 1** of UiO-67 Zr_6 nodes are compared with the EXAFS data in Table 2. Overall, the $Ir–O_t$ (O_t represents oxygen in terminal OH groups of a node) and Ir–C bond lengths obtained from DFT calculations agree well with the EXAFS data, to within 0.02 Å. The calculations however overestimate the Ir–Zr distances by 0.20 Å, consistent with the results reported for $Ir(CO)_2$ supported on NU-1000 (Table 2).[17] Moreover, the calculations show that the Ir atom is close to the oxygen atom of the bridging μ_3-OH (3.092 Å), while it is farther from the bridging μ_3-O group (4.156 Å). These results give an average Ir– O_b distance of 3.62 Å, agreeing within error with the EXAFS value of 3.45 Å (Table 2) and supporting the value of the coordination number of 2.1 for the $Ir–O_b$ structural parameter determined in the EXAFS data fitting.

Table 2. EXAFS structural parameters representing $Ir(C_2H_4)_2$ supported on UiO-67 Zr_6 nodes[a] and $Ir(CO)_2$ supported on NU-1000 Zr_6 nodes (data for NU-1000 from ref. 17).

		EXAFS				DFT
Sample	Shell	*N*	*R* (Å)	$10^3\times\Delta\sigma^2$ ($Å^2$)	ΔE_0 (eV)	*R* (Å)
$Ir(C_2H_4)_2$/UiO-67	Ir-Ir	[b]	[b]	[b]	[b]	
	$Ir–O_t$	2.1	2.15	9.8	6.7	2.13
	Ir–C	4.0	2.09	9.9	-4.2	2.09
	$Ir–O_b$	2.1	3.45	11.0	-0.7	3.62
	Ir–Zr	1.8	3.62	14.5	-3.5	3.82
$Ir(CO)_2$/NU-1000	Ir-Ir	[b]	[b]	[b]	[b]	
	$Ir–O_t$	2.0	2.05	5.4	-5.2	2.11
	$Ir–C_{co}$	2.1	1.97	14.6	-5.9	1.83
	$Ir–O_{co}$	2.1	2.99	14.5	7.4	2.98
	$Ir–O_b$	1.9	3.13	6.8	-5.6	3.39
	Ir–Zr	2.0	3.55	14.2	-0.7	3.72

[a]Notation: O_t, O atoms of terminal OH groups on Zr_6 node; C, ethylene carbon; O_b, O in bridging μ_3–OH or μ_3–O group on Zr_6 node; *N*, coordination number; *R*, distance between absorber and backscatterer atoms; $\Delta\sigma^2$, disorder term; ΔE_0, inner potential correction. Estimated EXAFS error bounds: *N*, ±20%; *R*, ±0.02 Å; $\Delta\sigma^2$, ±20%; ΔE_0, ±20% (errors characterizing the Ir−Zr contribution are greater); fit range: 3.85 < *k* (wave vector) < 13.61 $Å^{-1}$; 0.5 < *R* < 4 Å; goodness of fit value 2.5. [b]Contribution not detectable. Details of the EXAFS data fitting are as reported before.[17]

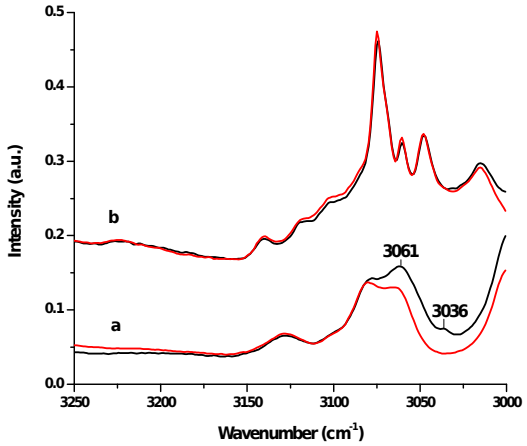

Figure 2. IR spectra in the ν_{CH} region characterizing the samples formed by adsorption of $Ir(C_2H_4)_2$(acac) on (a) UiO-66(HCl) and (b) UiO-67(HCl) (black) after it had been treated with a pulse of CO in helium for 3 min (red).

Groups on Zr_6 Nodes for Bonding Iridium Complexes. The modulators HCl and acetic acid provide control of the node sites that bond to the iridium complexes. The spectra of Figure 1 show that the hydroxyl band of **site 2** on UiO-66 and that of **site 1** on UiO-67 were greater in intensity when the modulator was HCl rather than acetic acid. In earlier work,[17] two types of bonding sites for metal complexes on UiO-66 were observed when the modulator was acetic acid. In contrast, only **site 2** defects were observed when the modulator was HCl. The results thus indicate that the topology of the Zr_6 node is markedly influenced by the modulator.

We infer that the topology of the Zr_6 node is also influenced by the type of solvent used for washing the MOF in the syntheses, because we observed both **site 1** and **site 2** when we used acetone instead of methanol to wash the HCl-modulated UiO-66 (Figure S7).

Because the HCl-modulated UiO-67 (washed with acetone) and NU-1000 (treated by HCl after synthesis and washed with acetone) are characterized by only **site 1** on their nodes, we further infer that the topology of the Zr_6 node is also influenced by the local structure of the pore and the crystal structure of the MOF.

The MOF nodes were further characterized by probing with reactive iridium complexes. Because the iridium complexes that became bonded to UiO-67(HCl) evidently consist of only one type of species, we took advantage of its simplicity to conduct the experiments described below—complemented by those with iridium complexes on

UiO-67(acetic acid), which consisted of mixed species.

Because UiO-67 modulated with acetic acid has far fewer defect sites than that modulated with HCl, adsorption of the same number of iridium complexes on each of these two MOFs (10 wt %) gave iridium complexes that were all chemisorbed on the nodes of UiO-67(HCl) but iridium complexes that were both physisorbed and chemisorbed on UiO-67(acetic acid) with its limited number of missing linker sites, as shown by the IR spectra. The results are consistent with the inference that the bonding sites for the metal complexes were the hydroxyl groups on the missing linker sites of the MOFs nodes.

Comparison of Reactivities of various MOF Node Sites with $Ir(C_2H_4)_2$(acac). When $Ir(C_2H_4)_2$(acac) reacted with UiO-66(HCl) having essentially all of the node surface sites present in the form of **site 2**, characterized by IR bands at 3692 and 3780 cm^{-1}, the intensity of the 3692 cm^{-1} band decreased significantly, and the 3780 cm^{-1} band disappeared, showing that the iridium complex reacted with these sites as it was chemisorbed. However, the intensities of the 3674 and 3644 cm^{-1} bands characterizing μ_3-OH groups remained essentially unchanged during the chemisorption, showing that, as the iridium complex reacted with the terminal hydroxyl groups of **site 2** of UiO-66, it did not react with bridging μ_3-OH groups.

In contrast, the reaction between $Ir(C_2H_4)_2$(acac) and UiO-67(HCl) and UiO-67(acetic acid)—with all of the node surface sites being **sites 1**, took place at these sites, as indicated by the decrease in intensity of the 2745 cm^{-1} band (Figures 1B and S1B). The bridging μ_3-OH group (characterized by bands at 3674 and 3642 cm^{-1}, Figure 1A) did not react with the organoiridium precursor.

IR spectra in the ν_{CH} region of the UiO-66(HCl)--supported sample (Figure 2) demonstrate the presence of ethylene ligands bonded to the iridium, as indicated by the bands at 3061 and 3036 cm^{-1}. These bands are assigned to ν_{CH} of π-bonded ethylene. The frequencies nearly match those of $Ir(C_2H_4)_2$ (acac).[23] These observations indicate that the ethylene ligands remained bonded to the iridium during the chemisorption.

The DFT calculations predict that the most intense ν_{CH} stretching modes of the ethylene ligands supported at the iridium center of **site 2** appear at approximately 3194 and 3172 cm^{-1}. The splitting of these calculated frequencies (22 cm^{-1}) matches the splitting in the experimental frequencies (25 cm^{-1}). Moreover, a scaling factor of 0.957 (close to the 0.956 that was determined in our previous work with $Ir(CO)_2$ species supported on NU-1000) reduces the mean unsigned error of the theoretical calculations to about 2.0 cm^{-1}.

The comparable IR experiments with the sample formed by adsorption of $Ir(C_2H_4)_2$(acac) on UiO-67(HCl) and UiO-67(acetic acid) provide much less information, because the bands characterizing the organic linkers in the range of 3000–3150 cm^{-1} are so intense that they would have swamped the weak bands characterizing the ethylene ligands; an equivalent statement pertains to UiO-67(acetic acid). The DFT calculations predict only marginal differences between the ν_{CH} stretching modes of $Ir(C_2H_4)_2$ supported at **site 1** and **site 2** of UiO-66.

EXAFS data characterizing the UiO-67-supported iridium complexes measured at the Ir L_{III} edge show no detectable Ir–Ir contributions, consistent with the inference that the supported iridium species were essentially mononuclear. The best fits of the data (Table 1) indicate that each Ir atom was bonded, on average, to two ethylene ligands as well as the two oxygen atoms of the support, as shown by the values of the Ir–C and Ir–O coordination numbers of nearly 4 and nearly 2, respectively. The data include an Ir–O_b and an Ir–Zr contribution with coordination numbers of 2.1 and 1.8 at distances of 3.45 and 3.62 Å, respectively, consistent with the IR data (Figure 1) and the inference that the iridium complexes were bonded at **site 1** of the Zr_6 node where a proton had been removed by the chemisorption.

Notwithstanding the aforementioned good agreement between the structural parameters obtained by EXAFS spectroscopy and DFT, there is some disagreement between the corresponding Ir–Zr distances (Table 2). A similar situation in which the calculated Ir–Zr distance overestimates the fitted EXAFS data by about 0.2–0.3 Å was encountered in our reported work on NU-1000,[17] consistent with the results of previous DFT/EXAFS investigations referred to before.[17] (We did not determine EXAFS data for the samples containing mixtures of chemisorbed and physisorbed iridium complexes because of the challenge of fitting such data for mixtures of species.)

Reaction of MOF Node-supported $Ir(C_2H_4)_2$ Complexes with CO. *Experimental evidence*. We used CO and IR spectroscopy to probe the supported iridium species. When the sample of $Ir(C_2H_4)_2$ supported on UiO-66(HCl) or on UiO-67(HCl) or UiO-67(acetic acid) was exposed to a pulse of CO at 298 K and 1 atm (~80 CO molecules per Ir atom), the initially π-bonded ethylene ligands in the supported $Ir(C_2H_4)_2$ complexes were readily replaced by CO, as shown, for example, by the disappearance of the IR bands at 3061 and 3036 cm^{-1} when the support was UiO-66(HCl) (Figure 2). Furthermore, the mass spectra of the effluent gas gave evidence of ethylene formed from each of these supported samples. There was a concomitant growth of ν_{CO} bands at 2074 and 1996 cm^{-1} (characterizing iridium complexes on **site 2**) when the support was UiO-66(HCl) and at 2066 and 1990 cm^{-1} (on **site 1**) when the support was UiO-67(HCl) or UiO-67(acetic acid) (Figure 3 and Figure S2). The spectra indicate chemisorbed iridium *gem*-dicarbonyls and demonstrate (with the lack of bridging carbonyl spectra) that the iridium species were mononuclear. The different

frequencies of the carbonyl bands are evidence of differences between the various MOF nodes as electron-donor ligands; this point is developed below.

We also detected physisorbed $Ir(CO)_2(acac)$ on UiO-66(HCl) and on UiO-67(acetic acid) after the CO treatments. The IR spectra show that in addition to the anchored iridium complexes, other iridium complexes were present that reacted with CO, as shown by the bands at 2085 and 2010 cm^{-1} (Figures 3 and S2).[17] We infer from the band locations that that physisorbed $Ir(C_2H_4)_2(acac)$ was present, and the changes in the spectra show that it was readily converted to $Ir(CO)_2(acac)$ when exposed to CO. The physisorbed species might have resided on the external MOF surfaces and/or been associated with the organic linkers.

Computational evidence. The reaction of CO with $Ir(C_2H_4)_2$ complexes supported on the Zr_6 nodes of UiO-66/67 and NU-1000 is suggested to proceed stepwise, as shown in reactions (1)–(3). Reactions (1)–(3) result in the formation of $Ir(C_2H_4)_2CO$ (**A**), $Ir(C_2H_4)CO$ (**B**), and $Ir(CO)_2$ (**C**). Reaction (4) depicts the overall exchange of two ethylene ligands with CO. The calculated free energy changes (ΔG) associated with these reactions at 298.15 K and 1.000 bar are presented in Table 3.

$$Ir(C_2H_4)_2 + CO \rightarrow Ir(C_2H_4)_2(CO) \quad (1)$$

$$Ir(C_2H_4)_2(CO) \rightarrow Ir(C_2H_4)(CO) \quad (2)$$

$$Ir(C_2H_4)(CO) + CO \rightarrow Ir(CO)_2 + C_2H_4 \quad (3)$$

and, overall,

$$Ir(C_2H_4)_2 + 2CO \rightarrow Ir(CO)_2 + 2C_2H_4 \quad (4)$$

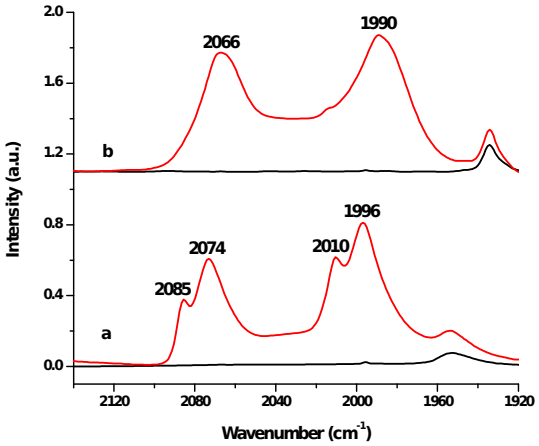

Figure 3. IR spectra in the ν_{CO} region characterizing the complexes initially present as $Ir(C_2H_4)_2$ complexes supported on (a) UiO-66(HCl) and on (b) UiO-67(HCl) in flowing helium (black) and after contact with a pulse of CO in helium at 298 K and 1 bar for 3 min (red).

Table 3. Calculated free energies (kcal/mol) of the reactions that occur when supported $Ir(C_2H_4)_2$ species react with CO gas.

	Site 1		Site 2
Reaction	NU-1000	UiO-66/67	UiO-66/67
(1)	-20.6	-20.1	-19.2
(2)	-0.9	-2.0	-2.6
(3)	-15.8	-15.6	-17.3
(4)	-37.3	-37.7	-39.2

The optimized structures of $Ir(C_2H_4)CO$ and $Ir(C_2H_4)_2$ are shown in Scheme 3. Our calculations show that overall reaction (4) is significantly exoergic, a result that is not surprising as CO is a stronger σ- and π-donor than C_2H_4.

The calculated frequencies of the C–O stretching vibrations in $Ir(CO)_2$ supported on UiO-66 were found to be 2165 and 2090 cm^{-1} for **site 1**, in contrast to 2173 and 2104 cm^{-1} for **site 2**.[17] The trends in the magnitude of these vibrational frequencies agree well with the empirical results presented in Figure 3. Indeed, application of a scaling factor of 0.956 reduces the mean unsigned error in the calculated values (relative to the experimental values) to about 4.2 cm^{-1}.

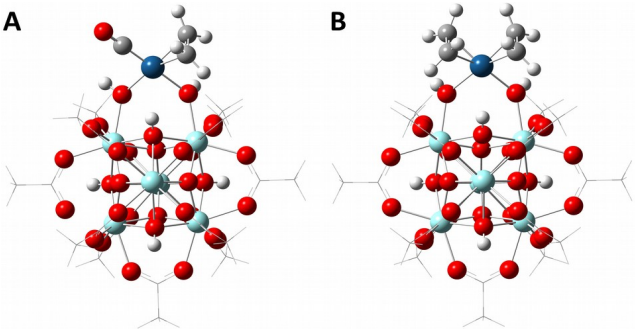

Scheme 3. Optimized structure of (A) the $Ir(C_2H_4)CO$ complex formed after exposure of UiO-66/67 node-supported $Ir(C_2H_4)_2$ complexes to CO and (B) UiO-66/67 node-supported $Ir(C_2H_4)_2$ complex.

Reactivities with ethylene of $Ir(CO)_2$ complexes on nodes of UiO-66 and of UiO-67. ***Experimental evidence.*** Further evidence of the electron-donor properties of the supports was determined in experiments characterizing the replacement of CO ligands on the iridium complexes with ethylene from a stream flowing at 298 K and 1 bar. Changes in the IR spectra in the ν_{CO} region occurred rapidly for both $Ir(CO)_2$ supported on UiO-66(HCl) and that supported on UiO-67(HCl); the initial iridium *gem*-dicarbonyl bands at 2074 and 1996 cm^{-1} characterizing the UiO-66-supported complexes and at 2066 and 1990 cm^{-1} characterizing the UiO-67-supported complexes decreased in intensity with time, with the simulta-

neous growing in of two bands, at 2038 and 2021 cm^{-1} for UiO-66-supported complexes, and the growing in of a band at 2021 cm^{-1} for the UiO-67-supported complexes.

The bands characterizing the UiO-66-supported species are assigned to $Ir(C_2H_4)_2(CO)$ and to $Ir(C_2H_4)(CO)$, respectively. These assignments are based on the results of a spectroscopic investigation of the zeolite HY-supported isostructural $Ir(CO)_2$ complexes and products formed from them when they were subjected to the same treatment conditions, whereby the initial ν_{CO} bands of $Ir(CO)_2$ on HY zeolite at 2038 and 2109 cm^{-1} shifted to 2054 and 2087 cm^{-1}; these are assigned to $Ir(C_2H_4)(CO)$ and $Ir(C_2H_4)_2(CO)$, respectively.[39] The band characterizing the UiO-67-supported species is assigned to $Ir(C_2H_4)(CO)$ on the basis of a similar comparison.[39]

Each of these new bands remained unchanged after 20 min of contact with ethylene (Figure 4). Estimates based on the band areas indicate that approximately 31% of the $Ir(CO)_2$ complexes supported on UiO-66(HCl) were converted to $Ir(C_2H_4)_x(CO)$ complexes, approximately 5% of these to $Ir(C_2H_4)_2(CO)$ and approximately 95% of these to $Ir(C_2H_4)(CO)$, and approximately 50% of the $Ir(CO)_2$ complexes supported on UiO-67(HCl) were converted to $Ir(C_2H_4)(CO)$. We tested the stabilities of the $Ir(C_2H_4)_x(CO)$ species by purging the IR cell with helium for 1 h. Figure 4B shows that the 2021 cm^{-1} band characterizing $Ir(C_2H_4)(CO)$ on UiO-67(HCl) decreased in intensity with time, disappearing after 30 min. Concurrently, the 2066 and 1990 cm^{-1} bands of $Ir(CO)_2$ on UiO-67(HCl) increased, indicating the conversion from $Ir(C_2H_4)(CO)$ to $Ir(CO)_2$ under helium.

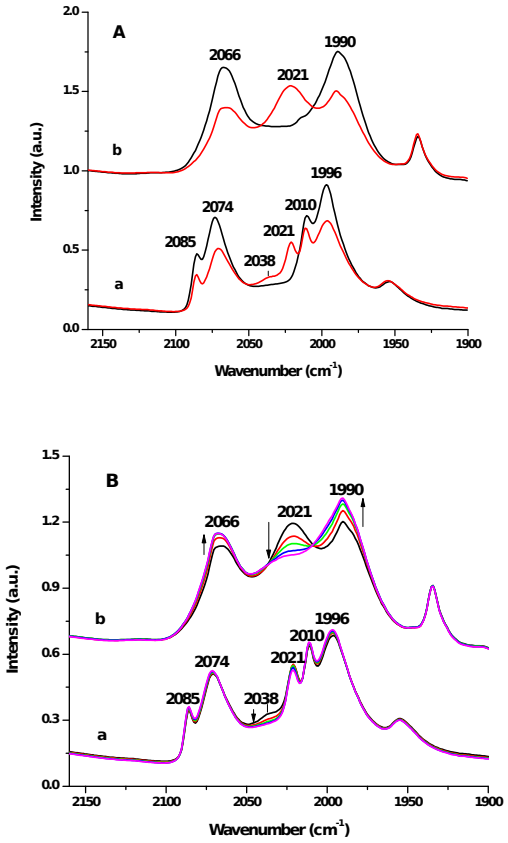

Figure 4. IR spectra in ν_{CO} region characterizing changes in the samples initially consisting of $Ir(CO)_2$ on (A) a, UiO-66(HCl) and b, UiO-67(HCl) after it had been exposed to flowing ethylene for 20 min at 298 K and 1 bar, (B) followed by flowing helium for 30 min. The $Ir(CO)_2$ complexes were prepared by treating the initial $Ir(C_2H_4)_2$ complexes with CO at 298 K.

In contrast, the 2021 cm^{-1} band characterizing $Ir(C_2H_4)(CO)$ on UiO-66 remained unchanged during a 30-min treatment in flowing helium, indicating that this species is quite stable on UiO-66(HCl). The weak band at 2038 cm^{-1} characterizing $Ir(C_2H_4)_2(CO)$ on UiO-66(HCl) gradually disappeared with the sample in flowing helium.

We emphasize that the physisorbed $Ir(CO)_2(acac)$ species represented by bands at 2085 and 2010 cm^{-1} did not react with ethylene. The reactivities of the iridium complexes anchored to the MOFs are compared in Table 3 with those of isostructural iridium complexes on other supports. For example, the $Ir(C_2H_4)_2(CO)$ species on UiO-66 are comparable in their reactivity to these complexes on dealuminated HY zeolite.

Computational evidence. As reactions (1)–(4) were all calculated as being exoergic (Table 3), we expect that an excess of ethylene would be required to drive them in the backward direction. Furthermore, we expect that removal of excess ethylene would result in the conversion of

$Ir(C_2H_4)_2(CO)$ and $Ir(C_2H_4)CO$ to $Ir(CO)_2$. These expectations concur with the experimental observations.

There is additional computational evidence for the exchange of CO with C_2H_4. First, the calculated CO stretching vibrational frequencies are 2084 cm^{-1} for $Ir(C_2H_4)CO$ and 2105 cm^{-1} for $Ir(C_2H_4)_2(CO)$, when we consider **site 1** of UiO-66/67. The DFT-calculated splitting between the vibrational frequencies of these species (21 cm^{-1}) agrees well with the experimental value (17 cm^{-1}). The theory and experiment also agree with respect to the trends in the magnitudes of the frequencies. Moreover, the calculated free energies of reaction (2) are low (-0.9 to -2.6 kcal/mol) and within the limits of error of DFT, thus not inconsistent with $Ir(C_2H_4)CO$ being more abundant than $Ir(C_2H_4)_2(CO)$.

Iridium complexes supported on ZrO_2. IR spectra of ZrO_2 (Figure S3) show a weak, sharp peak at 3739 cm^{-1} and a broad peak at 3676 cm^{-1}. These have been assigned to terminal OH and bridging μ_3-OH groups, respectively. After the chemisorption of $Ir(C_2H_4)_2(acac)$, the intensities of the 3739 cm^{-1} and 3676 cm^{-1} bands decreased markedly, indicating the reaction of this precursor with the OH groups (the terminal OH band was much weaker than the bridging OH band, and thus we infer that most of the reaction was with bridging OH groups). The bands of π-bonded ethylene ligands on iridium in this sample were too weak to discern (data not shown).

When the sample of $Ir(C_2H_4)_2$ supported on ZrO_2 was brought in contact with flowing CO, new ν_{CO} bands grew in, at 2061 and 1981 cm^{-1} (Figure S4). These bands are characteristic of iridium *gem*-dicarbonyls and indicate that the iridium species were mononuclear.

In contrast to the behavior of the UiO-66(HCl)- and UiO-67(HCl)-supported samples, the isostructural $Ir(CO)_2$ complexes supported on ZrO_2 were not reactive with ethylene under our conditions (Figure S5).

Comparison of MOF-supported iridium complexes as catalysts for ethylene conversion in the presence of H_2. The MOF-supported iridium complexes incorporating ethylene ligands were found to be precatalysts for the reactions of ethylene in the presence of H_2. Differential conversion data were obtained as a function of time on-stream in the flow reactor, with typical data shown in Figure S6; conversions were determined from the data showing the formation of products. The strategy and details of the experimentation are as described elsewhere.[36]

The conversions were extrapolated to zero time on-stream in order to provide measures of the initial activities of the (un-deactivated) catalysts. In the catalysis experiments, we used a low loading of iridium on all of the supports (1 wt %) to maximize the simplicity of the catalyst structures and to avoid the physisorbed iridium complexes formed on UiO-66(HCl) at a higher loading. Thus, at this low loading, chemisorbed iridium complexes were initially present solely on **site 2** of UiO-66(HCl), and chemisorbed iridium complexes were initially present solely on **site 1** of UiO-67(HCl) and NU-1000.

The conversion of ethylene in the presence of H_2 has been shown[42] to give the hydrogenation product, ethane—and, in the presence of some catalysts, butene isomers and butane indicating ethylene dimerization. The ethylene conversion has been investigated with iridium complexes on various supports, and a comparison of previously reported data with ours is given in Table 4. The earlier work[42] showed that the performance of catalysts comparable to ours for ethylene hydrogenation is strongly influenced by the support, with the reaction rate being much lower when the support is a good electron donor such as MgO than when it is a weak electron donor, such as dealuminated HY zeolite. The results summarized in Table 4 demonstrate that the selectivity for dimerization is also correlated with the electron-donor propriety of the support.

Our new results extend the observations to a family of supports that now includes metal oxides, zeolites, and MOFs.

Table 4. Structural characterization and catalyst performance data characterizing samples initially in the form of $Ir(C_2H_4)_2$ complexes on various supports. The data include characterization of the reaction of supported $Ir(C_2H_4)_2$ complexes to give supported $Ir(CO)_2$ complexes; the reactivities of supported $Ir(CO)_2$ complexes with C_2H_4; and catalytic activities for ethylene conversion in the presence of H_2 at 298 K and 1 bar[a]

Support[b]	ν_{CO} Band locations (cm^{-1})				Percentage of iridium complexes converted to $Ir(C_2H_4)(CO)$ when $Ir(CO)_2$ treated in flowing C_2H_4	Percentage of $Ir(CO)_2$ species converted to $Ir(C_2H_4)_x(CO)$ [c] when treated in flowing C_2H_4	Turnover frequency for ethylene conversion, TOF[d], s^{-1}	Selectivity in ethylene conversion, wt %[d]				
	$Ir(CO)_2$		$Ir(C_2H_4)_2(CO)$	$Ir(C_2H_4)(CO)$				ethane	*n*-butane	*trans*-2-butene	1-butene	*cis*-2-butene
HY zeolite	2109 (5)[e]	2038	2087	2054	60	100	0.60	95.0	0.6	2.3	0.8	1.3
UiO-66[f]	2074 (17)	1996	2038	2021	95	31	0.017	98.5	0.4	0.1	0.8	0.1
UiO-67[f]	2066 (33)	1990	n/a	2021	100	53	0.012	99.1	0.1	0.1	0.6	0.1
NU-1000	2066 (33)	1990	n/a	n/a	-	0	0.01	99.5	0[g]	0	0.5	0
ZrO_2	2061 (33)	1981	n/a	n/a	-	0	0.008	99.6	0[g]	0	0.4	0
MgO	2051 (26)	1967	n/a	n/a	-	0	0.003	100	0	0	0	0

[a]There was no detectable catalytic reaction in the absence of the catalyst under our conditions, and the supports alone were catalytically inactive; because some of the data reported previously were not collected under the same conditions as ours, all of the data reported in this table were obtained in this work, and the catalyst preparations were the same as those reported. [b]Support for catalyst initially incorporating node-anchored $Ir(C_2H_4)_2$. [c]Fractions of $Ir(C_2H_4)_x(CO)$, x = 1 or 2 species were estimated on the basis of the area under each peak in the ν_{CO} stretching region relative to the areas of the two ν_{CO} bands characterizing the respective $Ir(CO)_2$ species. [d]Turnover frequency calculated from differential conversions at time on stream = 0 and determined from ethylene conversions < 5%; catalyst mass: 30 mg; feed partial pressures: 100 mbar C_2H_4, 200 mbar H_2, 700 mbar helium; total flow rate 100 mL(NTP)/min; catalyst iridium content 1 wt %. [e]The numbers in parentheses are the full width at half-maximum (fwhm) values characterizing the carbonyl band. [f]MOFs were modulated with HCl. [g]Traces of butane were observed, but too small to quantify.

Discussion

Effect of MOF pore size on synthesis of supported iridium complexes. Figure 3 shows that chemisorption of the $Ir(C_2H_4)_2$ (acac) precursor was incomplete when the HCl-modulated UiO-66 was used as the support. The results are contrasted with those for iridium complexes supported on NU-1000 (reported previously[17]) and on HCl-modulated UiO-67, on which all of the iridium complexes were chemisorbed on the nodes. We emphasize that UiO-66(HCl) and UiO-67(HCl) have similar densities of bonding sites (~2.7 and 2.4 of the 12 sites per node, respectively, Table 1).

The results indicate mass transfer limitations in the chemisorption of the iridium complex on UiO-66. Comparable results were reported for the adsorption of $Rh(C_2H_4)_2$(acac) or $Ir(C_2H_4)_2$(acac) on the small-pore zeolite HSSZ-42—the pore opening of this zeolite is 6.4 × 6.4 Å, about the same as the critical diameters of the precursors (approximately 4 × 6 Å). Substantial adsorption evidently took place on the outer zeolite surface, forming physisorbed species, and we infer the same for UiO-66.

The ideal structure of UiO-66 has a pore aperture diameter of approximately 6 Å. The pore size of the HCl-modulated UiO-66 has been reported to be greater than that of the defect-free UiO-66,[20] because of missing linkers, but because the defects are randomly distributed in the MOF, the pores are expected to offer a tortuous path for mass transport, with a substantial transport restriction influencing the anchoring of the iridium complex.

In contrast, the pore aperture of UiO-67 is greater than that of UiO-66, about 8 Å,[18] and the pores of NU-1000 are even wider (with diameters of approximately 12 and 30 Å[16]). Thus, we infer that the iridium complexes readily entered the pores of the latter MOFs, without significant transport restrictions and therefore resulting in more nearly uniform distributions of iridium within the pore structures than in UiO-66—we would expect no gradients of iridium concentration in NU-1000.

Iridium species bonded to the nodes of UiO-66, UiO-67, and NU-1000. *Comparison of the nodes as electron donors.* The precursor $Ir(C_2H_4)_2$(acac) reacted with both **sites 1** and **sites 2** on the Zr_6 nodes of the three MOFs, leading to the dissociation of the acac ligand. The resulting $Ir(C_2H_4)_2$ complexes were found to be anchored to each of the nodes by two Ir–O_t (O_t is terminal oxygen in node **site 1** or **site 2**), as shown by the EXAFS data and DFT calculations (Table 2) and consistent with the IR spectra of the iridium *gem*-dicarbonyls formed from the iridium diethylene complexes on each node (Table 4).

The frequencies of the ν_{CO} bands are good indicators of the electron densities on the Ir atoms in the supported complexes. The available data (including literature data characterizing various metal oxide and zeolite supports, Table 4) indicate the following order of electron-donor strengths: MgO > ZrO_2 > UiO-67 (= NU-1000) > UiO-66 >> zeolite HY. The results indicate that **site 2** on UiO-66 has a lower electron-donor strength than **site 1** on UiO-67 or on NU-1000. The sites and nodes in UiO-67 and NU-1000 are essentially the same in structure, and, correspondingly, their electron-donor properties are essentially the same.

The ν_{CO} bands of iridium dicarbonyls on **site 1** or **site 2** of the Zr_6 nodes appeared at exactly the same frequencies even though the MOFs UiO-66 and UiO-67 modulated with acetic acid or HCl have significantly different numbers of defect sites per node. We thus infer that the electron-donor properties of **site 1** or **site 2** do not change significantly with the number of defect sites on the node.

As shown above, the calculated CO stretching frequencies reproduce the trends in the empirical results for **site 1** or **site 2** (and, when scaled, agree well with experiment).

Now we focus on another measure of the electron-donor properties of the iridium centers, the calculated partial charges on the iridium centers in the supported $Ir(CO)_2$ species. In our previous work, we found that for **site 1**, the calculated Mulliken partial charge is 0.36, much lower than that of **site 2**, 0.51. When we use the Hirshfeld charge analysis method, we find partial charges of 0.17 and 0.29 for **site 1** and **site 2**, respectively. These results support the conclusion that the iridium center at **site 2** has lower electron-donor strength than that at **site 1**. As previously noted, the calculated partial charges of the iridium centers are similar for **site 1** in UiO-66/67 and NU-1000.

To further check whether the density of ligand defects at each metal node affects the electron-donor strength of the anchored iridium centers, we optimized several structures for UiO-66/67, in which $Ir(CO)_2$ species were supported at 2 or 3 missing linker sites with H_2O/OH (**site 1**) pairs. In both cases (with 2 or 3 missing linkers), the partial atomic (Mulliken and Hirshfeld) charges of the iridium centers were the same within ± 0.04 as those determined when there was only one missing linker. The calculated ν_{CO} bands also remained largely unchanged (± 4.0 cm^{-1}). These results indicate that the facets of the Zr_6 nodes in NU-1000, UiO-66, and UiO-67 are well separated and are thus chemically almost identical, with only little variation in properties as a result of catalyst loading per node.

Comparison of reactivities of iridium complexes on various supports. The iridium dicarbonyl complexes on UiO-66 and on UiO-67 reacted with ethylene, leading to the displacement of one CO ligand per Ir atom and addition of one or two ethylene ligands. The data of Table 4 demonstrate that the reactivity of iridium dicar-

bonyl complexes with ethylene increased in the order MgO = ZrO_2 = NU-1000 (not reactive) < UiO-66 < UiO-67 << HY zeolite, indicating that for the most part the reactivity decreased with increasing electron-donor ability of the support. This pattern concurs with the calculated exoergicities of reactions (1)–(3), Table 3. $Ir(CO)_2$ supported at **site 2** in UiO-66 is less labile for CO exchange with ethylene than that at **site 1**.

However, significantly, the observed reactivities of $Ir(CO)_2$ complexes on the nodes of UiO-66, UiO-67, and NU-1000 with ethylene do not fall in line with the order of electron-donor properties determined by the frequencies of the aforementioned ν_{CO} bands. We infer that it would be oversimplifying matters to relate the reactivities of the supported iridium complexes just to the electron-donor properties of the supports that provide ligands. We suggest that the pore structures of the MOFs and the distributions of missing linkers on the Zr_6 nodes also influence the reactivity. The DFT calculations represent model clusters and are therefore not expected to capture these macroscopic effects.

$Ir(CO)(C_2H_4)_2$ species formed as minority species on UiO-66 but not on UiO-67, suggesting a greater ability of UiO-66 to coordinate multiple ligands and lower electron densities of the Ir atoms on UiO-66 than on UiO-67—in other words, a lower electron-donor tendency of UiO-66 than of UiO-67, consistent with the deduction from the calculated and empirical vibrational carbonyl stretching frequencies as well as the calculated atomic partial charges showing that **site 2** (present only in UiO-66) has a lower electron-donor strength than **site 1** (present in UiO-66, UiO-67, and NU-1000).

Furthermore, the carbonyl band of the Ir(CO)(C_2H_4) species on UiO-67 gradually decreased in intensity when the sample was present in flowing helium, indicating that ethylene ligands (or species formed from them, such as ethane formed in reactions of the ethylene ligands with hydrogen formed by reverse spillover from node OH groups[43]) desorbed. The simultaneous increase in intensity of the carbonyl bands of $Ir(CO)_2$ suggests the transfer of carbonyl ligands from one iridium complex to another. The Ir(CO)(C_2H_4) species on UiO-66 were found to be more stable than those on UiO-67 in flowing helium. The data may indicate that the higher electron-withdrawing tendency of UiO-66 helps stabilize the weakly bonded ethylene ligands.

Comparison of catalytic activities of iridium complexes on various supports. The data shown in Figure 5 indicate that the catalytic activities of the supported iridium complexes initially present as $Ir(C_2H_4)_2$ increased—both for ethylene hydrogenation and ethylene dimerization—as the iridium complexes became more electron-deficient. The support as a ligand influences the ability of iridium to bond with and activate the ligands formed from both ethylene and H_2.

The catalytic activities of $Ir(C_2H_4)_2$/UiO-66(HCl) summarized in Table 4 are the same as those of $Ir(C_2H_4)_2$/UiO-66(acetic acid) reported previously,[17] although these two MOFs are characterized by significantly different densities of node defect sites. The results indicate that the catalytic activity measured as a turnover frequency is barely if at all influenced by the number of defect sites in the MOF and that turnover frequency is an appropriate measure of catalytic activity. We emphasize that the activities of MOF-supported $Ir(C_2H_4)_2$ are determined by the types of bonding sites on the MOF nodes. Because **site 2** on UiO-66 has a lower electron-donor tendency than **site 1** on NU-1000 or on UiO-67, the iridium complexes on the former sites are more active than on the latter, consistent with the results presented in Table 3 and the results of DFT calculations reported in our previous work.[17]

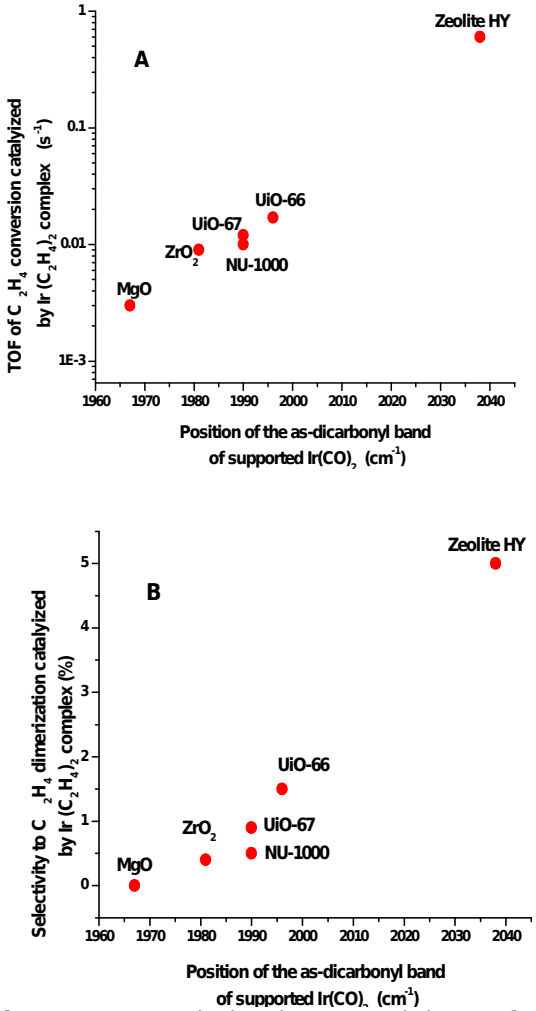

Figure 5. Correlation between (A) TOF for ethylene hydrogenation, and (B) selectivity for ethylene dimerization catalyzed by iridium complexes initially in the form of supported $Ir(C_2H_4)_2$ and ν_{CO} of the $Ir(CO)_2$ complexes formed from the cata-

lysts (a higher $\nu_{CO,as}$ frequency indicates that the iridium complex is more electron-deficient).

In contrast, zeolite HY-supported iridium complexes are characterized by much higher activity and selectivity for dimer formation than those supported on the MOFs with Zr_6 nodes. Work with supported rhodium complex catalysts for ethylene hydrogenation and dimerization at 298 K and 1 bar also indicated a strong influence of the support on the catalytic activity, showing that the rate of ethylene conversion is an order of magnitude higher when the support is zeolite HY than when it is MgO. In a further contrast between the electron-withdrawing zeolite and the electron-donating MgO, the selectivity for dimerization at our low conversions was found to be 80% when the support was zeolite HY, whereas no dimerization was observed when the support was MgO.

We have previously used DFT calculations to show that **site 2** on UiO-66 provides lower transition state barriers for ethylene hydrogenation and dimerization than **site 1** in UiO-66 and NU-1000.[17] It is therefore not surprising that UiO-67 and NU-1000 (two MOFs that possess only **sites 1**) have identical activities (Figure 5), whereas UiO-66 is more active for hydrogenation and dimerization, as a result of its more electropositive iridium centers at **site 2**.

It is however informative to consider whether a similar trend emerges from a comparison of the calculated CO band frequencies of metal *gem*-dicarbonyl species as well as the ν_{CH} stretching vibrational frequencies of $Ir(C_2H_4)_2$ species supported on a cluster model of HY zeolite. First, the asymmetric ν_{CH} stretching frequencies of C_2H_4 in HY zeolite-supported $Ir(C_2H_4)_2$ species (3174, 3185, 3213 and 3225 cm^{-1}) are higher than those on **site 1** (3171, 3172, 3194, and 3194 cm^{-1}) or **site 2** (3180, 3182, 3199, and 3201 cm^{-1}) of UiO-66. Correspondingly, the calculated Ir–C bond lengths in the zeolite-supported species (2.08 Å) are slightly less than those in the UiO-66/67- or NU-1000-supported species (2.09 Å). These results would suggest that iridium supported on HY zeolite binds/activates C_2H_4 more strongly than that in the isostructural species on **sites 1** and **2** on the three MOFs. However, the calculated CO frequencies of $Ir(CO)_2$ supported on the HY zeolite cluster (2174 and 2103 cm^{-1}) are similar to those obtained for $Ir(CO)_2$ on **site 2** of UiO-66 (2174 and 2104 cm^{-1}), suggesting similarities between them.

Degrees of uniformity of bonding sites on various supports. The ν_{CO} band of *gem*-dicarbonyls of iridium on ZrO_2, UiO-67, and UiO-66 have full width at half-maximum (fwhm) values of approximately 33, 33, and 17 cm^{-1}. A reported value characterizing iridium *gem*-dicarbonyls bonded to the nodes of NU-1000 is 33 cm^{-1}.[17] The fwhm values of iridium *gem*-dicarbonyls on HY zeolite and on MgO have been reported to be 5 and 26 cm^{-1}, respectively. These values indicate that the degree of uniformity of the iridium species on these supports increased in the order of ZrO_2 ≈ UiO-67 ≈ NU-1000 < MgO < UiO-66 << HY zeolite.

The fwhm of the carbonyl band of $Ir(C_2H_4)(CO)$ on UiO-67 is markedly greater than that of the carbonyl band of $Ir(C_2H_4)(CO)$ on UiO-66 (Figure 4), indicating that **sites 1** on UiO-67 nodes are less nearly uniform than **sites 2** on UiO-66 nodes. Thus, the node bonding sites vary from one MOF in the family considered here to another with respect to their degree of uniformity.

Comparison of nodes of UiO-66, UiO-67, and NU-1000 with ZrO_2. Bulk ZrO_2 calcined at 773 K is represented by a broad IR band centered at 3676 cm^{-1}, assigned to bridging μ_3–OH groups, and this frequency is close to that of the bridging μ_3-OH groups on these Zr_6 nodes. The iridium complexes are observed (Figure S3) to bond at these μ_3–OH groups on bulk ZrO_2, but instead to the non-hydrogen bonded terminal OH or hydrogen-bonded H_2O/OH groups of the MOFs that contain Zr_6 nodes—μ_3-OH groups on the MOFs do not react substantially with the organoiridium precursor under our conditions. DFT calculations confirm that the reaction of iridium complexes with μ_3-OH groups is endoergic by 28 kcal/mol, much more than the value characterizing the reaction of iridium complexes bonding with **site 1** (-4.3 kcal/mol) and **site 2** (1.2 kcal/mol).[17] The frequencies of the ν_{CO} bands of the iridium dicarbonyls bonded to these supports are indicators of the poorer electron-donor tendency of the MOF nodes than of bulk ZrO_2, corresponding to higher reactivities and catalytic activities of the MOF node-supported iridium complexes.

Comparison of UiO-66, UiO-67, and NU-1000 with zeolites as ligands and catalyst supports. To repeat, the degree of uniformity of the various supported iridium complexes is indicated by the sharpness of the ν_{CO} bands in the IR spectra. Non-uniform bonding sites on the support surfaces give broader ν_{CO} bands in the iridium *gem*-dicarbonyl spectra of the complexes on MOFs than on zeolites, which are characterized by narrow bands, with fwhm values of typically 5 cm^{-1}.[36] Our observations demonstrate that the MOF nodes present more nearly uniform sites than metal oxides, and also that there are differences from one MOF to another (Table 3), but the data show that each of the MOFs offers sites that are much less nearly uniform than the sites on zeolite HY.

The origins of the heterogeneity of the MOF node sites may be a consequence in part of mobility of the hydrogen atoms on the various bonding sites. These hydrogen atoms can bridge two terminals O sites or just be located on one. This variety in bonding of the hydrogen is evidenced by the following observations: after reaction with iridium

complexes, **sites 1** on both UiO-67 and NU-1000 with two hydrogen atoms on each bonding site have similar degrees of uniformity, whereas they are both less uniform than **sites 2** on UiO-66, which has only one hydrogen on a bonding site. In contrast, bonding of an iridium complex to the zeolite may remove most of the zeolite protons (which react to form Hacac), contributing to the relatively high degree of uniformity of the zeolite-supported iridium complexes.

These points remain to be clarified. The issues are important for evaluation of the prospects of applying MOF nodes as catalyst supports; because the MOF node structures are almost molecular in character and have relatively high degrees of uniformity, they are good candidates for bonding of catalytic groups guided by theory.[17]

Zeolite HY-supported $Ir(C_2H_4)_2$ complexes have been found to provide entry to new chemistry of metal complexes, including activation of H_2 at 298 K leading to formation of iridium hydrides[48] and formation of reactive iridium-dinitrogen complexes.[49] We infer that, at least in part, because the three Zr_6-containing MOF nodes investigated here had weaker electron-withdrawing tendencies than zeolite HY, the rich chemistry occurring on iridium complexes on the zeolite was not observed in this work.

Nonetheless, modified MOF node compositions might be expected to open up more possibilities for new reactivities.[16] Improvement in syntheses may lead to MOF nodes with higher degrees of uniformity than those reported here, and new MOFs might offer improved opportunities for highly selective catalysts associated with highly uniform structures. Many of the reactions observed with zeolite-supported metal complexes take place in association with acidic sites on the zeolites, especially Brønsted acidic sites. The Zr_6-containing MOFs have hydroxyl groups that are Brønsted acids, but they are weakly acidic. Thus, discovery of MOFs with nodes that resemble acidic zeolites or metal oxides may be expected to lead to new opportunities for the application of MOFs in catalysis.

CONCLUSIONS

Molecular $Ir(C_2H_4)_2$ complexes bonded to the Zr_6-containing nodes of the MOFs UiO-66, UiO-67, and NU-1000 have been compared with isostructural complexes bonded to metal oxides and zeolites. The UiO-66 used in this work was synthesized to contain only node sites for bonding of iridium complexes that consisted of non-hydrogen bonded terminal OH groups (**site 2**), whereas our UiO-67 and NU-1000 had node sites consisting only of hydrogen-bonded H_2O/OH groups (**site 1**). The data reported here demonstrate that electron-donor tendencies of the MOF nodes and metal oxide and zeolite supports decrease in the order MgO > ZrO_2 > UiO-67 (= NU-1000) > UiO-66 >> zeolite HY. The supports are ligands for the metal complexes and influence the electron densities of the metal's valence orbitals, which affect its ability to coordinate multiple ligands and its reactivity and catalytic activity and selectivity for reactions exemplified by ethylene hydrogenation and ethylene dimerization. The degree of uniformity of **site 2** on UiO-66 is greater than that of **site 1** on UiO-67 or on NU-1000, and the latter MOFs in this respect resemble bulk, powder ZrO_2, but all of the MOF node-supported iridium complexes are much less nearly uniform than those on zeolite HY.

As in our previous work, we show that DFT calculations can be used to provide detailed insights into the structure, reactivity, and catalytic properties of iridium catalysts bonded to the nodes of NU-1000, UiO-66, and UiO-67. The calculated ν_{CO} and ν_{CH} stretching frequencies of the iridium *gem*-dicarbonyl, $Ir(CO)_2$, and iridium diethylene species, $Ir(C_2H_4)_2$, are in good agreement with empirical results. The calculated results are crucial for identifying the locations/sites of the iridium catalysts in the MOFs. Our calculations also show that the reactivity of the CO ligands on supported $Ir(CO)_2$ sites with ethylene reflects the electron-donor properties of the iridium sites, which in turn, are reflected by the calculated (and observed) ν_{CO} stretching frequencies and the calculated partial atomic charges. These relationships between the electronic structures of the supported iridium sites and the catalytic activities for ethylene hydrogenation and dimerization point to the possibilities for designing catalysts in which the metal site is modified by introduction of either additional electron-withdrawing ligands or co-adsorbed metal centers. We envisage that the metal sites in such catalysts may be synthesized to be more or less electron-deficient and consequently more active and/or selective for target reactions.

ASSOCIATED CONTENT

Supporting Information. Experimental and details are reported, primarily IR spectra. This material is available free of charge via the Internet at http://pubs.acs.org.

AUTHOR INFORMATION

Corresponding Authors

* bcgates@ucdavis.edu (B.C.G.)
* gagliard@umn.edu (L.G.)

Notes

The authors declare no competing financial interests.

ACKNOWLEDGMENT

This work was supported as part of the Inorganometallic Catalyst Design Center, an Energy Frontier Research Center funded by the U.S. Department of Energy (DOE), Office of Science, Basic Energy Sciences (BES), under Award DE-SC0012702.

REFERENCES

(1) Furukawa, H.; Cordova, K. E.; O'Keeffe, M.; Yaghi, O. M. *Science* **2013**, *341*, 1230444/1-12.
(2) Ferey, G. *Chem. Soc. Rev.* **2008**, *37*, 191-214.
(3) Horike, S.; Shimomura, S.; Kitagawa, S. *Nat. Chem.* **2009**, *1*, 695-704.
(4) Corma, A.; Garcia, H.; Xamena, F. X. L. I. *Chem. Rev.* **2010**, *110*, 4606-4655.
(5) Lee, J.; Farha, O. K.; Roberts, J.; Scheidt, K. A.; Nguyen, S. T.; Hupp, J. T. *Chem. Soc. Rev.* **2009**, *38*, 1450-1459.
(6) Gascon, J.; Corma, A.; Kapteijn, F.; Xamena, F. X. L. I. *ACS Catal.* **2014**, *4*, 361-378.
(7) Farrusseng, D.; Aguado, S.; Pinel, C. *Angew. Chem. Int. Edit.* **2009**, *48*, 7502-7513.
(8) Dhakshinamoorthy, A.; Alvaro, M.; Garcia, H. *Catal. Sci. Technol.* **2011**, *1*, 856-867.
(9) Ma, L. Q.; Abney, C.; Lin, W. B. *Chem. Soc. Rev.* **2009**, *38*, 1248-1256.
(10) Yoon, M.; Srirambalaji, R.; Kim, K. *Chem. Rev.* **2012**, *112*, 1196-1231.
(11) Manna, K.; Zhang, T.; Carboni, M.; Abney, C. W.; Lin, W. B. *J. Am. Chem. Soc.* **2014**, *136*, 13182-13185.
(12) Fei, H. H.; Cohen, S. M. *J. Am. Chem. Soc.* **2015**, *137*, 2191-2194.
(13) Gonzalez, M. I.; Bloch, E. D.; Mason, J. A.; Teat, S. J.; Long, J. R. *Inorg. Chem.* **2015**, *54*, 2995-3005.
(14) Larabi, C.; Quadrelli, E. A. *Eur. J. Inorg. Chem.* **2012**, 3014-3022.
(15) Nguyen, H. G. T.; Schweitzer, N. M.; Chang, C. Y.; Drake, T. L.; So, M. C.; Stair, P. C.; Farha, O. K.; Hupp, J. T.; Nguyen, S. T. *ACS Catal.* **2014**, *4*, 2496-2500.
(16) Mondloch, J. E.; Bury, W.; Fairen-Jimenez, D.; Kwon, S.; DeMarco, E. J.; Weston, M. H.; Sarjeant, A. A.; Nguyen, S. T.; Stair, P. C.; Snurr, R. Q.; Farha, O. K.; Hupp, J. T. *J. Am. Chem. Soc.* **2013**, *135*, 10294-10297.
(17) Yang, D.; Odoh, S. O.; Wang, T. C.; Farha, O. K.; Hupp, J. T.; Cramer, C. J.; Gagliardi, L.; Gates, B. C. *J. Am. Chem. Soc.* **2015**, *137*, 7391-7396.
(18) Cavka, J. H.; Jakobsen, S.; Olsbye, U.; Guillou, N.; Lamberti, C.; Bordiga, S.; Lillerud, K. P. *J. Am. Chem. Soc.* **2008**, *130*, 13850-13851.
(19) Schaate, A.; Roy, P.; Godt, A.; Lippke, J.; Waltz, F.; Wiebcke, M.; Behrens, P. *Chem. Eur. J.* **2011**, *17*, 6643-6651.
(20) Katz, M. J.; Brown, Z. J.; Colon, Y. J.; Siu, P. W.; Scheidt, K. A.; Snurr, R. Q.; Hupp, J. T.; Farha, O. K. *Chem. Commun.* **2013**, *49*, 9449-9451.
(21) Serna, P.; Gates, B. C. *Acc. Chem. Res.* **2014**, *47*, 2612-2620.
(22) Wu, H.; Chua, Y. S.; Krungleviciute, V.; Tyagi, M.; Chen, P.; Yildirim, T.; Zhou, W. *J. Am. Chem. Soc.* **2013**, *135*, 10525-10532.
(23) Bhirud, V. A.; Uzun, A.; Kletnieks, P. W.; Craciun, R.; Haw, J. F.; Dixon, D. A.; Olmstead, M. M.; Gates, B. C. *J. Organomet. Chem.* **2007**, *692*, 2107-2113.
(24) Odoh, S. O.; Cramer, C. J.; Truhlar, D. G.; Gagliardi, L. *Chem. Rev.* **2015**, *115*, 6051-6111.
(25) Perdew, J. P.; Burke, K.; Ernzerhof, M. *Phys. Rev. Lett.* **1996**, *77*, 3865-3868.
(26) Grimme, S.; Antony, J.; Ehrlich, S.; Krieg, H. *J. Chem. Phys.* **2010**, *132*, 154104/1-18.
(27) Kresse, G.; Furthmuller, *J. Phys. Rev. B* **1996**, *54*, 11169-11186.
(28) Kresse, G.; Furthmuller, *J. Comp. Mater. Sci.* **1996**, *6*, 15-50.
(29) Blochl, P. E. *Phys. Rev. B* **1994**, *50*, 17953-17979.
(30) Planas, N.; Mondloch, J. E.; Tussupbayev, S.; Borycz, J.; Gagliardi, L.; Hupp, J. T.; Farha, O. K.; Cramer, C. J. *J. Phys. Chem. Lett*. **2014**, *5*, 3716-3723.
(31) Zhao, Y.; Truhlar, D. G. *J. Chem. Phys.* **2006**, *125*, 194101/1-17.
(32) Metz, B.; Stoll, H.; Dolg, M. *J. Chem. Phys.* **2000**, *113*, 2563-2569.
(33) Weigend, F. *Phys. Chem. Chem. Phys.* **2006**, *8*, 1057-1065.
(34) Weigend, F.; Ahlrichs, R. *Phys. Chem. Chem. Phys.* **2005**, *7*, 3297-3305.
(35) Alecu, I. M.; Zheng, J. J.; Zhao, Y.; Truhlar, D. G. *J. Chem. Theory Comput.* **2010**, *6*, 2872-2887.
(36) Uzun, A.; Bhirud, V. A.; Kletnieks, P. W.; Haw, J. F.; Gates, B. C. *J. Phys. Chem. C* **2007**, *111*, 15064-15073.
(37) Mihaylov, M.; Ivanova, E.; Thibault-Starzyk, F.; Daturi, M.; Dimitrov, L.; Hadjiivanov, K. *J. Phys. Chem. B* **2006**, *110*, 10383-13185.
(38) Solymosi, F.; Novak, E.; Molnar, A. *J. Phys. Chem* **1990**, *94*, 7250-7255.
(39) Lu, J.; Aydin, C.; Liang, A. J.; Chen, C. Y.; Browning, N. D.; Gates, B. C. *ACS Catal.* **2012**, *2*, 1002-1012.
(40) He, M. Y.; Ekerdt, J. G. *J. Catal.* **1984**, *87*, 381-388.
(41) Ma, Z. Y.; Cheng, Y.; Wei, W.; Li, W. H.; Sun, Y. H. *J. Mol. Catal. A* **2005**, *227*, 119-124.
(42) Lu, J.; Serna, P.; Aydin, C.; Browning, N. D.; Gates, B. C. *J. Am. Chem. Soc.* **2011**, *133*, 16186-16195.
(43) Uzun, A.; Gates, B. C. *J. Am. Chem. Soc.* **2009**, *131*, 15887-15894.
(44) Lu, J.; Aydin, C.; Browning, N. D.; Gates, B. C. *Langmuir* **2012**, *28*, 12806-12815.
(45) Serna, P.; Gates, B. C. *J. Am. Chem. Soc.* **2011**, *133*, 4714-4717.
(46) Yardimci, D.; Serna, P.; Gates, B. C. *Chem. Eur. J.* **2013**, *19*, 1235-1245.
(47) Uzun, A.; Ortalan, V.; Browning, N. D.; Gates, B. C. *J. Catal.* **2010**, *269*, 318-328.
(48) Lu, J.; Aydin, C.; Browning, N. D.; Gates, B. C. *J. Am. Chem. Soc.* **2012**, *134*, 5022-5025.
(49) Yang, D.; Chen, M. Y.; Martinez-Macias, C.; Dixon, D. A.; Gates, B. C. *Chem. Eur. J.* **2015**, *21*, 631-640.

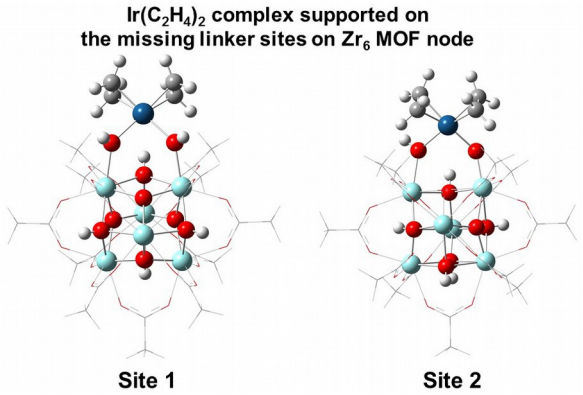
Ir(C2H4)2 complex supported on
the missing linker sites on Zr6 MOF node
Site 1
Site 2

TOC artwork